CELL BIOLOGY

Cevipabulin-tubulin complex reveals a novel agent binding site on α-tubulin with tubulin degradation effect

Jianhong Yang[1]*[†], Yamei Yu[1][†], Yong Li[1][†], Wei Yan[1][†], Haoyu Ye[1], Lu Niu[1], Minghai Tang[1], Zhoufeng Wang[2], Zhuang Yang[1], Heying Pei[1], Haoche Wei[1], Min Zhao[1], Jiaolin Wen[1], Linyu Yang[1], Liang Ouyang[1], Yuquan Wei[1], Qiang Chen[1], Weimin Li[2]*, Lijuan Chen[1]*

Microtubules, composed of αβ-tubulin heterodimers, have remained popular anticancer targets for decades. Six known binding sites on tubulin dimers have been identified thus far, with five sites on β-tubulin and only one site on α-tubulin, hinting that compounds binding to α-tubulin are less well characterized. Cevipabulin, a microtubule-active antitumor clinical candidate, is widely accepted as a microtubule-stabilizing agent by binding to the vinblastine site. Our x-ray crystallography study reveals that, in addition to binding to the vinblastine site, cevipabulin also binds to a new site on α-tubulin. We find that cevipabulin at this site pushes the αT5 loop outward, making the nonexchangeable GTP exchangeable, which reduces the stability of tubulin, leading to its destabilization and degradation. Our results confirm the existence of a new agent binding site on α-tubulin and shed light on the development of tubulin degraders as a new generation of antimicrotubule drugs targeting this novel site.

INTRODUCTION

Microtubules play key roles in many important cell events, especially cell division, and remain as one of the most popular anticancer targets for decades (1, 2). Microtubules are composed of αβ-tubulin heterodimers assembled into linear protofilaments, and their packaging demands both lateral and longitudinal interactions between tubulins (3). To date, various tubulin inhibitors have been reported to alter the lateral and/or longitudinal interactions to promote microtubule assembly or disassembly, including the clinically most popular anticancer drugs: vinca alkaloids, taxanes, eribulin, etc. (4, 5). These drugs all target β-tubulin, which has five different binding sites (colchicine, vinblastine, paclitaxel, laulimalide, and maytansine sites) (5). By overexpression of β-tubulin isoforms, especially βIII-tubulin, cancer cells are prone to become resistant to these therapies (6). So far, the pironetin site is the only one located on α-tubulin (5, 7), but this site is too small, and pironetin has six chiral centers in its molecular structure, making it difficult to be synthesized. Since the crystal structure of the tubulin-pironetin complex was reported in 2016 (5, 7), no notable progress has been made in the design of pironetin-binding-site inhibitors or even analog of pironetin.

Tubulin inhibitors are functionally divided into two categories: microtubule stabilization agents (MSAs) and microtubule destabilization agents (MDAs). MSAs that promote microtubule polymerization include the paclitaxel and laulimalide site inhibitors, and structure biological studies reveal that they both stabilize the M loop to enhance lateral interactions to promote tubulin polymerization (8, 9). MDAs that inhibit microtubule polymerization contain the colchicine, vinblastine, maytansine, and pironetin site inhibitors.

Colchicine binds to intradimer interfaces to prevent tubulin dimers from adopting a "straight conformation," thereby inhibiting lateral interactions (10). Maytansine and pironetin bind to the interdimer interfaces to inhibit longitudinal interactions (5, 7, 11), and vinblastine also binds to the interdimer interfaces but acts as a wedge to enhance abnormal longitudinal interactions and eventually self-associate into spiral aggregates (3). Recently, some tubulin degradation agents, such as T0070907, T007-1, and withaferin A, have been reported (12, 13), but their degradation mechanism remains unclear.

Cevipabulin (or TTI-237) is a synthetic tubulin inhibitor with in vivo anticancer activity and has been used in clinical trials investigating the treatment of advanced malignant solid tumors (14). Competition experiment showed that it competed with ³H-vinblastine, but not ³H-paclitaxel, for binding to microtubules, indicating that it binds to the classic tubulin-depolymerization vinblastine site (15). However, an in vitro tubulin polymerization assay exhibited that cevipabulin did not inhibit tubulin polymerization as vinblastine but promoted tubulin polymerization as paclitaxel (15). These studies concluded that cevipabulin seems to be displaying mixed properties between paclitaxel and vinblastine. Kovalevich et al. (16) have found that cevipabulin could promote tubulin degradation. However, the degradation mechanism was not fully elucidated. Recently, Saez-Calvo et al. synthetized an analog of cevipabulin (named compound 2 in this paper) and obtained the crystal structure of the compound 2–tubulin complex [Protein Data Bank (PDB) code: 5NJH]. They proved that compound 2 binds to the vinblastine site of β-tubulin, enhancing longitudinal interactions that induce the formation of tubulin bundles in cells, and further confirmed that compound 2 binds to the vinblastine site to induce tubulin polymerization in a paclitaxel-like manner (17).

In this study, we further investigate the tubulin-inhibition mechanism of cevipabulin. Our crystal structure of the cevipabulin-tubulin complex reveals that cevipabulin simultaneously binds to two spatially independent sites: the vinblastine site and a new site on α-tubulin (called the seventh site). Biochemical experiments confirm that the binding of cevipabulin to the new site is responsible

[1]Laboratory of Natural and Targeted Small Molecule Drugs, State Key Laboratory of Biotherapy and Cancer Center, National Clinical Research Center for Geriatrics, West China Hospital, Sichuan University and Collaborative Innovation Center of Biotherapy, Chengdu 610041, China. [2]Department of Respiratory Medicine, West China Hospital, Sichuan University, Chengdu 610041, China.
*Corresponding author. Email: chenlijuan125@163.com (L.C.); weimi003@yahoo.com (W.L.); yjh1988@scu.edu.cn (J.Y.)
†These authors contributed equally to this work.

for its tubulin degradation effect. Our study reveals a novel binding site on α-tubulin related to tubulin degradation effect and lays a foundation for the rational design of new generation of anti-cancer drugs.

RESULTS

Cevipabulin induces tubulin-heterodimer degradation

Cevipabulin was found to down-regulate tubulin protein level in different cells (*16*). To elucidate the cellular effect of cevipabulin at an early time point, we carried out label-free quantitative proteomic analysis on a 6-hour cevipabulin-treated human cervical adenocarcinoma cell line HeLa. Cevipabulin significantly down-regulated the protein level of α-tubulin, β-tubulin, and their isoforms with high selectivity (Fig. 1A). Immunoblotting study confirmed that cevipabulin decreased tubulin proteins in HeLa, human colon colorectal carcinoma cell line Hct116, human large cell lung carcinoma cell line H460, and human B cell lymphoma cell SU-DHL-6 in a dose-dependent (Fig. 1B) and time-dependent manner in HeLa cells (Fig. 1C), demonstrating that the reduction of tubulin was a common biochemical consequence of cevipabulin treatment in cancer cells. The quantitative PCR assay showed that cevipabulin had no effect on α- and β-tubulin mRNA levels (Fig. 1D), indicating

that the down-regulation of tubulin protein treated by cevipabulin was posttranscriptional. *N*-carbobenzyloxy-L-leucyl-L-leucyl-L-leucinal (MG132), a proteasome inhibitor, could completely block cevipabulin-induced tubulin degradation (Fig. 1E). All these proved that cevipabulin promotes tubulin degradation in a proteasome-dependent pathway.

Crystal structure of cevipabulin-tubulin reveals its simultaneous binding to the vinblastine site and a novel site on α-tubulin

Previous studies concluded that cevipabulin was an MSA binding to the vinblastine site (*14*, *18*). However, the detailed interaction between tubulin and cevipabulin was not elucidated. To analyze the binding details of cevipabulin (Fig. 2A) to tubulin, we soaked cevipabulin into the crystals consisting of two tubulin heterodimers, one stathmin-like protein RB3 and one tubulin tyrosine ligase (T2R-TTL) (*8*). The crystal structure of the cevipabulin-tubulin complex was determined to be 2.6 Å resolution (Table 1). The whole structure was identical to that previously reported (*8*), in which two tubulin heterodimers were arranged in a head-to-tail manner (α1β1-α2β2) with the long helix RB3 comprising both dimers and TTL docking onto α1-tubulin (Fig. 2B). The F_{obs}/F_{calc} (observed and calculated structure factor, respectively) difference electron density
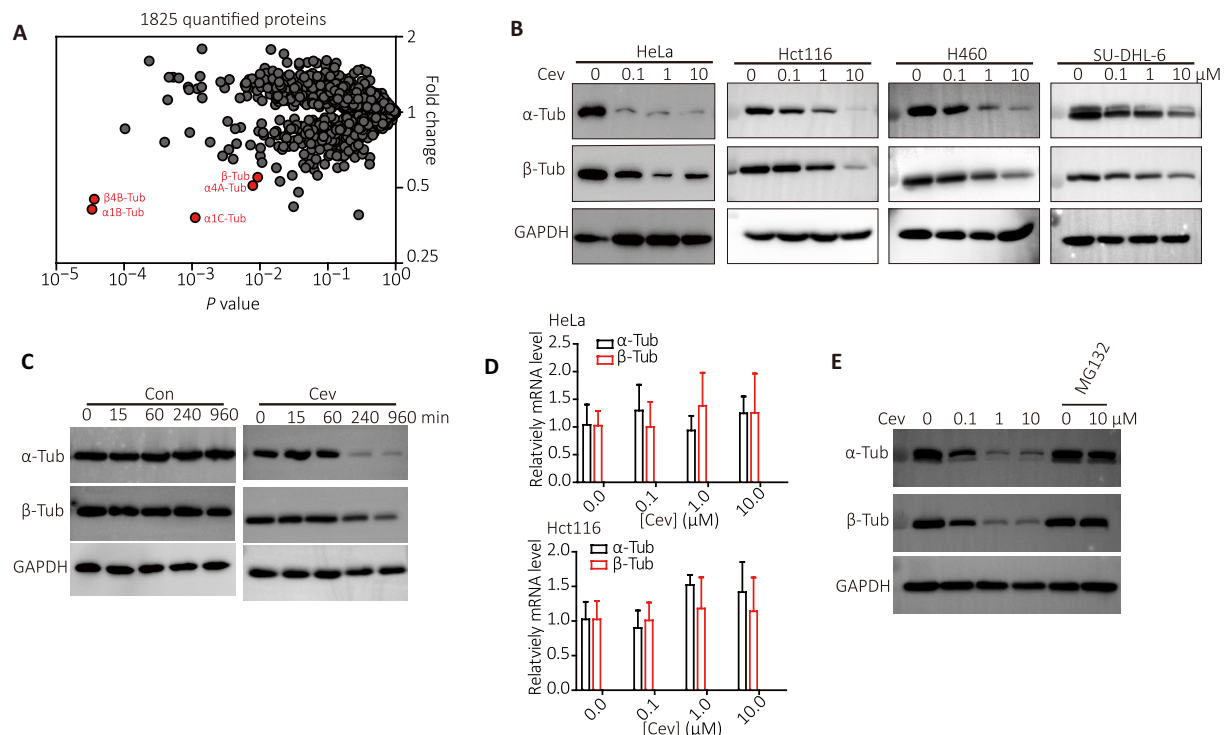

Fig. 1. Cevipabulin promotes tubulin dimer degradation. (**A**) Label-free quantitative proteomic analysis of total proteins from HeLa cells treated with 1 μM cevipabulin for 6 hours. This graph presents fold changes of 1825 quantified proteins between cevipabulin and DMSO treatment groups versus the *P* value (*t* test; triplicate analysis). Three biological repetitions are performed. (**B**) Immunoblotting analysis of both α- and β-tubulin levels in HeLa, Hct116, H460, and SU-DHL-6 cells, which all are treated with indicated concentrations of cevipabulin for 16 hours. Results are representative of three independent experiments. (**C**) HeLa cells were treated with 1 μM cevipabulin for the indicated times, and then the α- and β-tubulin levels were detected by immunoblotting. Results are representative of two independent experiments. (**D**) HeLa and Hct116 cells were treated with indicated concentrations of cevipabulin for 16 hours, and then mRNA levels of both α-tubulin and β-tubulin were measured by quantitative-PCR. Data were shown as means ± SD of three independent experiments. (**E**) Cells were treated with or without MG132 (20 μM) for 1 hour before treated with different concentrations of cevipabulin for 16 hours. Protein levels of both α- and β-tubulin were detected by immunoblotting. Results are representative of two independent experiments. Cev, cevipabulin; Tub, tubulin.
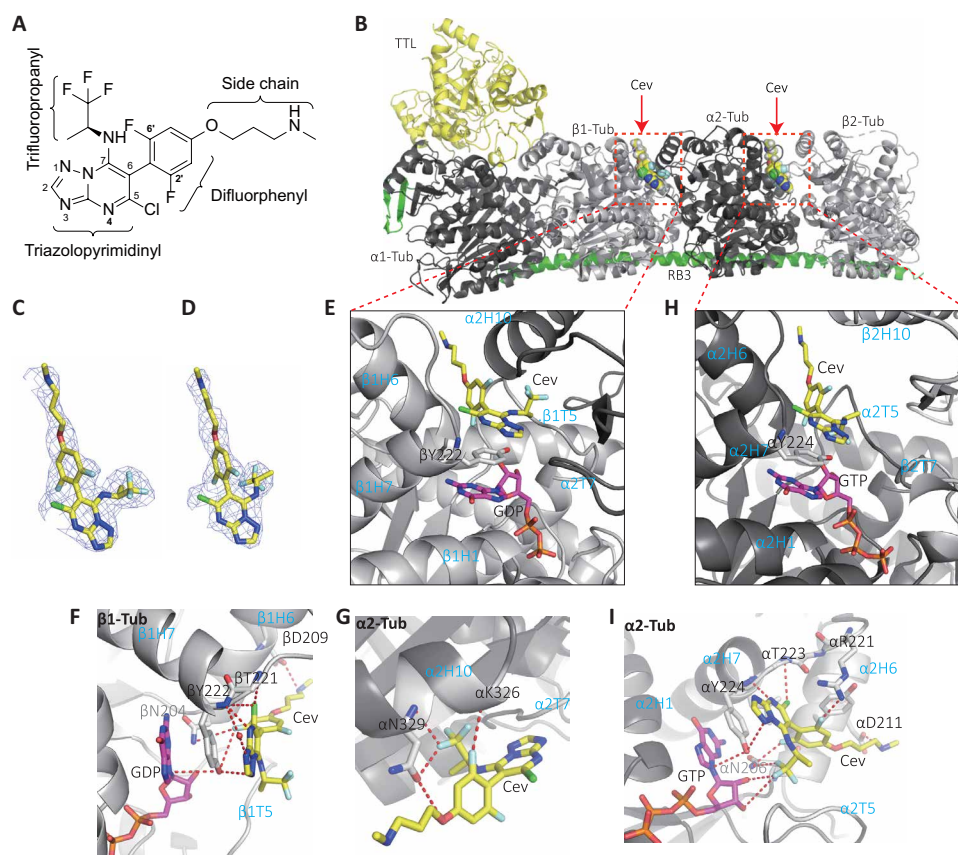
Fig. 2. Crystal structure of the cevipabulin-tubulin complex. (**A**) Chemical structure of cevipabulin. (**B**) Overall structure of the cevipabulin-tubulin complex. TTL is colored yellow, RB3 is green, α-tubulin is black, and β-tubulin is gray. Cevipabulin on β1-tubulin and α2-tubulin are all shown in spheres and colored yellow. (**C** and **D**) Electron densities of cevipabulins on (C) β1-tubulin or (D) α2-tubulin. The F_{obs}/F_{calc} omit map is colored light blue and contoured at 3δ. (**E** to **G**) Close-up view of vinblastine-site cevipabulin binding to (E and F) β1-tubulin or (G) α2-tubulin. GDP or GTP is shown in magenta sticks. Cevipabulin is shown in yellow sticks. Side chain of β1-Y224 or α2-Y224 is shown in gray sticks. (**H**) Interactions between the seventh-site cevipabulin and α2-tubulin. Color coding is the same as in (E). Residues from tubulin that form interactions with vinblastine-site cevipabulin are shown as sticks and labeled. Hydrogen bonds are drawn with red dashed lines. (**I**) Interactions between α2-tubulin and the seventh-site cevipabulin; Color coding is the same as in (F); residues from tubulin that form interactions with the seventh-site cevipabulin are shown as sticks and labeled. Hydrogen bonds are drawn with red dashed lines. Cev, cevipabulin.

unambiguously revealed two cevipabulin molecules binding to two different sites (Fig. 2, C and D): one at the interdimer interfaces between the β1- and α2-tubulin subunits (the vinblastine site) and the other one at the intradimer interfaces between α2- and β2-tubulin subunits (Fig. 2B), and the latter binding region is a new binding site (here named as the seventh site).

The binding region of cevipabulin in the vinblastine site was formed by residues from βH6, βH7, and βT5 loops and αH10 and αT7 loops (Fig. 2E). As presented in Fig. 2F, the side chain of βY222 made π-π stacking interactions with the triazolopyrimidinyl group of cevipabulin and the guanine nucleobase of guanosine diphosphate (GDP). Seven hydrogen bonds (N1 atom to the side chain of βY222, N3 atom to the main-chain nitrogen of βY222 through water, N4 atom to the main-chain nitrogen of βY222, 5-chlorine atom to both the main-chain nitrogen of βY222 and βT221, and 2′-fluorine atom to the side chain of βY222 and the main-chain nitrogen of βN204) between cevipabulin and β1-tubulin were observed. The -NH- group on the cevipabulin side chain formed a salt bridge with βD209. Besides, cevipabulin also exhibited four hydrogen bonds

with α2-tubulin (oxygen atom to the side chain of αN329, 2′-fluorine atom to the main-chain nitrogen of αN326, and one fluorine atom of trifluoropropanyl to both the main-chain and side chain of αN326) (Fig. 2G).

The seventh site on α2-tubulin is formed by residues from αH1, αH6, αH7, and αT5 (Fig. 2H). Similar to the vinblastine site, triazolopyrimidinyl of cevipabulin at this site also made π-π stacking interactions with the side chain of αY224 and the guanine nucleobase of guanosine 5′-triphosphate (GTP) (Fig. 2I). There were eight hydrogen bonds (N1 atom to the side chain of αY224, N4 atom to the main-chain nitrogen of αY224, 5-chlorine atom to the main-chain nitrogen of αT223, 2′-fluorine atom to the side chain of αN206, 6′-fluorine atom to the side chain of αR221, one fluorine atom of trifluoropropanyl to the side chain of αN206, and another fluorine atom of trifluoropropanyl to both O2′ and O3′ of GTP) between cevipabulin and α2-tubulin and a salt bridge between the -NH- group of the cevipabulin side chain and αD211 (Fig. 2I). Notably, there is no hydrogen bond between cevipabulin and β2-tubulin at this new site.

Table 1. Data collection and refinement statistics.

	Cevipabulin-tubulin	Cevipabulin-eribulin-tubulin
Data collection		
Space group	$P2_12_12_1$	$P2_12_12_1$
Cell dimensions		
a, b, c (Å)	104.4, 160.8, 174.8	103.9, 159.0, 176.2
α, β, γ (°)	90.0, 90.0, 90.0	90.0, 90.0, 90.0
Resolution (Å)	50.0–2.60 (2.64–2.60)*	89.5–2.45 (2.49–2.45)*
R_{pim} (%)	3.1 (42.2)	2.7 (37.1)
$I/\sigma I$	23.6 (2.0)	24.3 (2.0)
Completeness (%)	100 (100)	95.1 (100)
Redundancy	13.4 (13.0)	12.8 (13.9)
Refinement		
Resolution (Å)	50.0–2.61	59.5–2.45
No. of reflections	83,938	102,877
R_{work}/R_{free} (%)	20.7/25.8	22.7/26.4
No. of atoms		
Protein	17,464	17,489
Ligand/ion	241	349
Water	294	118
B factors		
Protein	44	54
Ligand/ion	56	76
Water	54	48
r.m.s. deviations		
Bond lengths (Å)	0.008	0.005
Bond angles (°)	0.789	0.851
Ramachandran (%)		
Favored	97.10	96.50
Outliers	0.05	0.05

*Highest-resolution shell is shown in parenthesis.

Direct biochemical assay confirms the binding of cevipabulin to the vinblastine site and the seventh site of tubulin

To ensure that the new binding site is not an artifactual interaction due to highly concentrated environment of the crystal, we further measured the binding of cevipabulin to the tubulin heterodimer in solution (without the other proteins used to obtain crystals). Tubulin (20 μM) in solution was incubated with different concentrations of cevipabulin, and the content of bound cevipabulin was collected and quantified by liquid chromatography–tandem mass spectrometry (LC-MS/MS). As shown in Fig. 3A, at respectively 64, 128, and 256 μM concentrations of cevipabulin, the stoichiometry was 1.74, 1.91, and 2.19 cevipabulin molecule per tubulin dimer, suggesting the formation of a 2:1 cevipabulin-tubulin complex. Since eribulin is a strong tubulin inhibitor binding to the microtubule plus ends (the vinblastine site) and can keep tubulin dimers in an assembly-incompetent dimer state (*4*), to confirm that cevipabulin simultaneously binds to the vinblastine site and the new binding site, we first blocked the vinblastine site with excessive eribulin before incubating with different concentrations of cevipabulin, and then the contents of both bound eribulin and cevipabulin were collected and quantified by LC-MS/MS. As shown in Fig. 3B, at 24, 48, and 96 μM cevipabulin, respectively, we observed that each tubulin dimer binds approximately one cevipabulin and one eribulin molecule, suggesting the formation of a 1:1:1 cevipabulin-eribulin-tubulin complex. Using the eribulin-incubated tubulin, we could directly measure the dissociation constant (K_d) of cevipabulin to the seventh site by a microscale thermophoresis assay (MST). As presented in Fig. 3C, the MST results showed that the K_d of cevipabulin to the seventh site is 0.97 ± 0.15 μM. We also solved the crystal structure of the cevipabulin-eribulin-tubulin complex using the T2R-TTL crystal. As shown in Fig. 3D, we clearly observed one molecule of cevipabulin binding on β1-tubulin, one molecule of cevipabulin on α2-tubulin, and one molecule of eribulin on β2-tubulin. Focusing
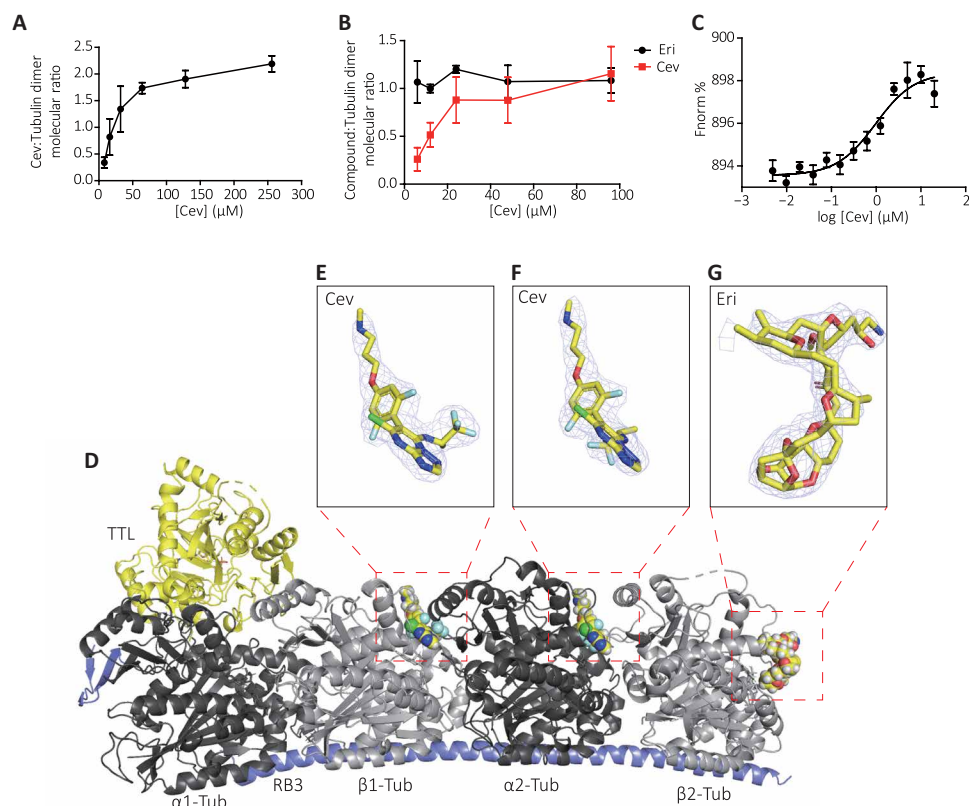
Fig. 3. Measuring the binding stoichiometry of cevipabulin to tubulin. (**A**) Indicated concentrations of cevipabulin were incubated with tubulin (20 μM) for 10 min, and then the bound cevipabulin was quantified by LC-MS/MS. This graph presented the molecular ratio of the cevipabulin:tubulin dimer. Data were shown as means ± SD of three independent experiments. (**B**) Indicated concentrations of cevipabulin were incubated with the eribulin-tubulin complex (20 μM) for 10 min, and then the bound cevipabulin and eribulin were quantified by LC-MS/MS. This graph presented the molecular ratio of the cevipabulin:tubulin or eribulin:tubulin dimer. Data were shown as means ± SD of three independent experiments. (**C**) Binding of cevipabulin to the seventh site of tubulin was determined with the microscale thermophoresis assay. Data points represent means ± SD of three technical replicates each. (**D**) Structure of the cevipabulin-eribulin-tubulin complex. TTL is colored yellow, RB3 is blue, α-tubulin is black, and β-tubulin is gray. Cevipabulin on β1-tubulin and α2-tubulin and eribulin on β2-tubulin were all shown in spheres and colored yellow. (**E** to **G**) Electron densities of cevipabulin on β1-tubulin (E) or α2-tubulin (F) and eribulin on β2-tubulin (G). The F_{obs}/F_{calc} omit map is colored light blue and contoured at 3δ. Cev, cevipabulin; Eri, eribulin; Tub, tubulin.

on the α2β2-tubulin dimer, we obtained a 1:1:1 cevipabulin-eribulin-tubulin complex, which was consistent with the results of our biochemical experiments. Next, we carried out the competition experiments of cevipabulin to boron-dipyrromethene (BODIPY)-vinblastine to measure the K_d value of cevipabulin to the vinblastine site, which is determined to be 0.90 ± 0.24 μM (fig. S1, A and B). All these results confirmed that, in addition to the vincristine site, cevipabulin could simultaneously bind to the seventh site.

Cevipabulin binding to the seventh site to induce tubulin degradation

We then investigated whether the new binding site of cevipabulin to tubulin mediated tubulin degradation. When vinblastine site was occupied by eribulin or vinblastine, cevipabulin retains the tubulin-degradation effect (Fig. 4A and fig. S2A). Since the αY224 at the seventh site forms π-π stacking interactions with the triazolopyrimidinyl group of cevipabulin and the guanine nucleobase of GTP, it may be important for the binding of cevipabulin. Thus, single amino acid substitution (Y224G on α-tubulin) was used to block the seventh site. When the seventh site was mutant, cevipabulin lost its

ability to degrade tubulin (Fig. 4B). These data indicated that cevipabulin binding to the seventh site rather than vinblastine binding plays a role in the degradation of tubulin. To further understand the underlying degradation mechanism, we synthesized two reported cevipabulin analogs [compounds **1** (*16*) and **2** (*17*)] (Fig. 4C). Compared with cevipabulin, compound **1** has no N-substituted side chain, and the trifluoropropanyl in compound **1** was replaced by an azabicyclo to obtain compound **2**. As exhibited in Fig. 4D, compound **1** induced tubulin degradation, while compound **2** did not. LC-MS/MS results indicated that compound **1** bound to tubulin dimer with a 1:1 stoichiometry, and MST assay conformed compound **1** to bind to eribulin preincubated tubulin with a K_d value of 14.91 ± 1.23 μM (Fig. 4E and fig. S2B). Further experiments indicated that αY224G mutation, but neither vinblastine nor compound **2**, inhibited compound **1**–induced tubulin degradation (Fig. 4F and fig. S2, C and D). These results together demonstrated that either cevipabulin or compound **1** binding to the seventh site induced tubulin degradation, while compound **2** only binding to vinblastine did not induce tubulin degradation, suggesting that the trifluoropropyl of cevipabulin plays a key role for binding to this new site.
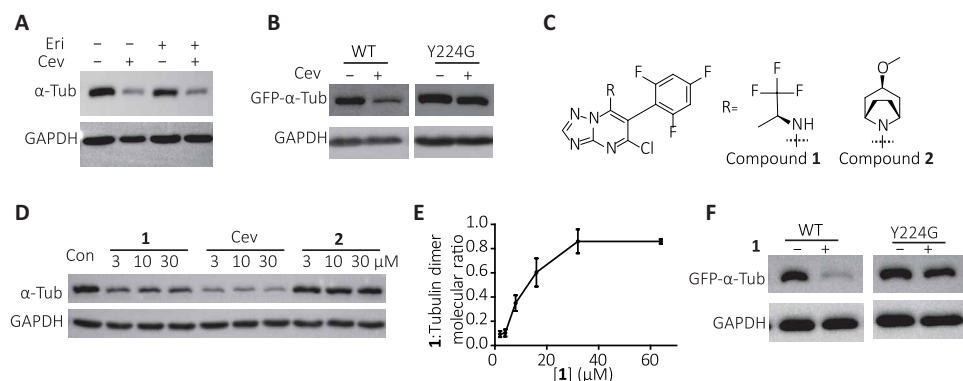
Fig. 4. Cevipabulin binds to the seventh site to induce tubulin degradation. (**A**) HeLa cells were treated with 10 μM eribulin for 1 hour and then further treated with 1 μM cevipabulin for 16 hours. The α-tubulin protein level was detected by immunoblotting. Results are representative of three independent experiments. (**B**) Vectors expressing either wild-type (WT) or Y224G mutant GFP-tubulin were transfected to HeLa cells. After 24 hours, cells were treated with or without 1 μM cevipabulin for 16 hours. Then, the protein level of GFP-α-tubulin was detected by immunoblotting. Results are representative of three independent experiments. (**C**) Chemical structure of cevipabulin derivatives. (**D**) HeLa cells were treated with indicated compounds for 16 hours. Then, the protein level of α-tubulin was detected by immunoblotting. Results are representative of three independent experiments. (**E**) Indicated concentrations of compound **1** were incubated with tubulin (20 μM) for 10 min, and then the bound compound **1** was quantified by LC-MS/MS. This graph presented the molecular ratio of the compound **1**:tubulin dimer. Data were shown as means ± SD of three independent experiments. (**F**) Vectors expressing either wild-type or Y224G mutant GFP-tubulin were transfected to HeLa cells. After 24 hours, cells were treated with or without 10 μM compound **1** for 16 hours. Then, the protein level of GFP-α-tubulin was detected by immunoblotting. Results are representative of three independent experiments. Cev, cevipabulin; **1**, compound **1**; **2**, compound **2**; Vin, vinblastine.

Cevipabulin and compound 1 destabilize tubulin by making the nonexchangeable GTP exchangeable

Crystal structures of cevipabulin-tubulin and compound **2**–tubulin (PDB code: 5NJH) could be superimposed very well in whole (with a root mean square deviation of 0.45 Å over 1930 Cα atoms; fig. S3A) or in the vinblastine-site region (fig. S3B). Thus, the main conformational change of cevipabulin-tubulin is identical to compound **2**–tubulin, which has been described in detail in a previous study (*17*), except for the presence of additional density at the seventh site. We then focus on the study of this novel site. The nonexchangeable GTP plays a structural role and is important for the stability of tubulin dimers (*19*, *20*). As tubulin degradation induced by cevipabulin is mediated by its binding to the seventh site located near the nonexchangeable GTP, we suspect that cevipabulin and compound **1** may directly mediate the stability of tubulin. Using a thiol probe, tetraphenylethene maleimide (TPE-MI), which is nonfluorescent until conjugated to a thiol (Fig. 5A) (*21*), we measured whether these compounds promote unfolding of tubulin. As shown in Fig. 5B, TPE-MI alone did not increase fluorescence of tubulin, while addition of 4 M guanidine hydrochloride (nonselective protein denaturant) significantly increased fluorescence. Cevipabulin and compound **1** obviously increased tubulin fluorescence, while vinblastine and compound **2** had no such effects, demonstrating that cevipabulin or compound **1** could promote unfolding of tubulin. In the seventh site, the α-T5 loop undergoes a large outward shift after binding to cevipabulin (Fig. 5C), resulting in the destruction of some important hydrogen bonds between the nonexchangeable GTP and α-T5 loop (Fig. 5D), which we believe may affect the affinity of GTP to α-tubulin protein. We then incubated tubulin with different compounds for 10 min in buffer containing 1 mM GDP, and then the contents of tubulin-bound GTP and GDP were detected by LC-MS/MS. As shown in Fig. 5F, compared with the control groups, the contents of GTP decreased, and GTP increased after treatment with cevipabulin or compound **1**, while both the contents of GTP and GDP did not change after treatment with

compound **2** or vinblastine, suggesting that cevipabulin or compound **1** binding reduces the affinity of this nonexchangeable GTP to α-tubulin and eventually makes it exchangeable. Therefore, the degradation process can be summarized as follows: Cevipabulin or compound **1** binds at the seventh site and pushes the α-T5 loop outward, breaking some important hydrogen bonds between α-T5 and the nonexchangeable GTP, reducing the affinity between GTP and α-tubulin, thereby reducing tubulin stability and promoting its destabilization and degradation.

DISCUSSION

Our study identifies a novel binding site on α-tubulin, named as the seventh site of tubulin. As this new site is located near the nonexchangeable GTP site, which is important for tubulin stability (*19*, *20*, *22*), inhibitors such as cevipabulin and compound **1** binding to the seventh site reduce tubulin stability and promote tubulin degradation. This novel site on α-tubulin spatially corresponds to the vinblastine site on β-tubulin, which is also bound by cevipabulin. Binding pockets of cevipabulin to the two sites are very similar (formed by αH1, αH6, αH7, and αT5 for the seventh site and βH1, βH6, βH7, βT5, αH10, and αT7 for the vinblastine site), and the binding modes of cevipabulin are also similar, except the trifluoropropanyl of cevipabulin adopts different conformations. Vinblastine-site cevipabulin is mainly located on β1-tubulin and forms lots of hydrogen bonds with β1-tubulin, while its trifluoropropanyl is oriented toward α2-tubulin and makes four hydrogen bond interactions with α2-tubulin. The seventh site cevipabulin is totally located on α2-tubulin, forming a number of hydrogen bonds with α2-tubulin, and its trifluoropropanyl is also oriented toward α2-tubulin to establish hydrogen bonds with the nonexchangeable GTP. Compound **2**, lacking the trifluoropropanyl, could not bind to the seventh site and showed no tubulin degradation effect, suggesting that the trifluoropropanyl-GTP interaction is important for cevipabulin binding to the seventh site. We noticed that in the
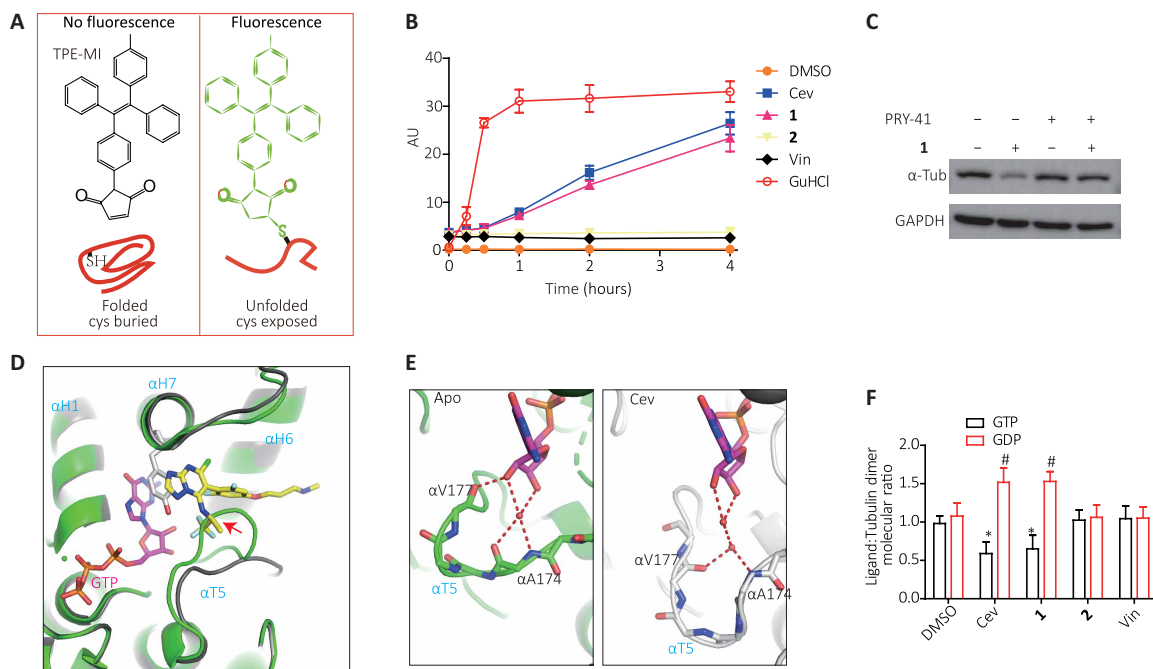
Fig. 5. Cevipabulin or compound 1 decreases tubulin stability to promote tubulin destabilization and degradation. (**A**) The fluorescence of TPE-MI is enabled upon conjugation to a cysteine residue of a denatured protein. (**B**) Tubulin unfolding detected by TPE-MI. Tubulin was mixed with TPE-MI, and the indicated compounds for various times before fluorescence were detected ($n = 3$). (**C**) HeLa cells were treated with or without PYR-41 for 1 hour before treated with compound **1** for 16 hours. Protein level of α-tubulin was detected by immunoblotting. Results are representative of three independent experiments. (**D**) Close-up view of the seventh site in the cevipabulin-tubulin (black) and apo-tubulin (green, PDB code: 4i55) complex that were aligned on α2-tubulin. GTP, magenta sticks; cevipabulin, yellow sticks; side chain of α2-Y224, gray sticks. The collision of the α-T5 loop in the apo-tubulin complex to cevipabulin is marked with a red arrow. (**E**) Close-up view of the interaction between the nonexchangeable GTP and the α-T5 loop in the apo-tubulin (left) or the cevipabulin-tubulin (right) complex. Main chain of the α-T5 loop, sticks. Hydrogen bonds, red dashed lines. (**F**) Tubulin in buffer supplemented with 1 mM GDP was incubated with indicated compounds; both bound GTP and GDP were further quantified. Molecular ratio of the GTP:tubulin or GDP:tubulin dimer was shown. Data were presented as means ± SD of three independent experiments. *$P < 0.05$ (GTP) or #$P < 0.05$ (GDP), compound content as compared to the DMSO-treated group. Cev, cevipabulin; Vin, vinblastine; **1**, compound **1**; **2**, compound **2**. AU, arbitrary units.

compound **2**–tubulin complex (PDB code: 5NJH), although compound **2** bound only to the vinblastine site, the αT5 loop at the seventh site also had an outward shift as in the cevipabulin-tubulin complex (fig. S4A), and there is weak but clear density at the new site in the crystallographic maps of 5NJH (fig. S4B). It seems to suggest that compound **2** could also bind to the seventh site but with much lower affinity. However, biochemical results indicated that compound **2** showed no interaction with the seventh site at low micromolar concentrations (*17*), and compound **2** cannot induce tubulin degradation. Although we confirmed that compound **1** binds only to the seventh site and not to the vinblastine site, we unfortunately did not obtain the crystal structure of the tubulin–compound **1** complex (possibly because of the lower affinity of compound **1** to the seventh site), which might provide other vital information on the seventh site.

To prove that the binding of cevipabulin to the seventh site was not an artifactual interaction caused by the high concentration of the crystal environment or as a result of crystal packing or an artifact of T2R-TTL protein complex used, we measured the binding in solution (without the RB3 and TTL protein used for crystallization) at micromolar concentration. We observed that 20 μM tubulin dimer in solution could be bound with 40 μM cevipabulin at most, suggesting the formation of a 2:1 cevipabulin-tubulin complex. In addition, when the vinblastine site was blocked by a strong tubulin inhibitor—eribulin, 20 μM tubulin dimer can still be bound with

20 μM cevipabulin and forms a 1:1:1 cevipabulin-eribulin-tubulin complex. All these demonstrated that cevipabulin can bind to the seventh site at low micromolar concentration, and an MST assay directly determined the K_d of cevipbulin to the seventh site (eribulin-tubulin complex) to be 0.97 ± 0.15 μM. We further soaked both cevipabulin and eribulin simultaneously to the T2R-TTL complex to obtain a cevipabulin-eribulin-tubulin complex. We observed one molecule of cevipabulin on α2-tubulin and one molecule of eribulin on β2-tubulin (Fig. 2D), indicating the formation of a 1:1:1 cevipabulin-eribulin-tubulin complex, which is consistent with the biochemical results. We found one molecule of cevipabulin but not eribulin on β1-tubulin, suggesting that cevipabulin has much higher affinity to the interdimer-face vinblastine site than eribulin. Thus, though these two compounds both bind to the vinblastine site, eribulin preferred to bind to the vinblastine site at the plus end, while cevipabulin only binds to the interdimer-face vinblastine site with high affinity.

The novel site is located near the nonexchangeable GTP, which plays a structural role and is important for the stability of tubulin dimers (*19*, *20*). This nonexchangeable GTP forms a number of hydrogen bonds with surrounding amino acid residues and a magnesium ion (*19*). Single mutation abolishing the hydrogen bond with this GTP could reduce the affinity of GTP, and the absence of the magnesium ion would reduce the protein stability (*19*, *22*). Cevipabulin binds to the new site and pushes the α-T5 loop outward, breaking

several key hydrogen bonds, reducing the nonexchangeable to α-tubulin, and promoting its unfolding, thereby inducing its degradation in a proteasome-dependent pathway. Therefore, compounds bound to the seventh site of tubulin may all induce tubulin degradation because the α-T5 loop outward shift was necessary for compounds binding.

Here, we have reported a novel binding site on α-tubulin that had a tubulin degradation effect that was distinct from the traditional MDAs and MSAs. Using this specific site, a new class of tubulin degraders can be designed as anticancer drug targeting α-tubulin.

MATERIALS AND METHODS

Reagents
Colchicine, vinblastine, BODIPY-vinblastine, β,γ-methyleneadenosine 5′-triphosphate disodium salt (AMPPCP), TPE-MI, and DL-dithiothreitol (DTT) were purchased from Sigma-Aldrich; eribulin mesylate was obtained from MOLNOVA. Guanidine hydrochloride, MG132, and PYR-41 were obtained from Selleckchem; cevipabulin was from MedChemExpress; purified tubulin was bought from Cytoskeleton Inc.; and antibodies [α-tubulin, β-tubulin, glyceraldehyde-3-phosphate dehydrogenase (GAPDH), and gout anti-mouse secondary antibodies] were bought from Abcam.

Chemistry
All the chemical solvents and reagents used in this study were analytically pure without further purification and commercially available. Thin-layer chromatography (TLC) was performed on 0.20-mm silica gel 60 F_{254} plates (Qingdao Ocean Chemical Factory, Shandong, China). Visualization of spots on TLC plates was done by ultraviolet light. Nuclear magnetic resonance (NMR) data were measured for ^{1}H at 400 MHz on a Bruker Avance 400 spectrometer (Bruker Company, Germany) using tetramethylsilane as an internal standard (IS). Chemical shifts were quoted in parts per million. High-resolution mass spectra (HRMS) were recorded on a Q-TOF (quadrupole orthogonal acceleration–time-of-flight) Bruker Daltonics model IMPACT II mass spectrometer (Micromass, Manchester, UK) in a positive mode. Brief synthesis procedures of compounds **1** and **2** are shown in fig. S5.

General procedure for the synthesis of diethyl 2-(2,4,6-trifluorophenyl)malonate (5)
To a stirred solution of diethyl malonate (320 mg, 2.0 mmol) in 1,4-dioxane was added 60% sodium hydride (96 mg, 2.4 mmol) by portions at room temperature. Then, copper(I) bromide (380 mg, 2.0 mmol) and compound **4** (211 mg, 1.0 mmol) were added. The reaction mixture was stirred at room temperature for 30 min and then refluxed for 8 hours under nitrogen protection. After completion of the reaction, the mixture was cooled to room temperature and hydrochloric acid (12 N, 50 ml) was added slowly. The organic phase was separated off, and the aqueous phase was extracted with ethyl acetate (×2). The combined organic phase was concentrated in vacuo. The residue was purified by chromatography on silica gel with petroleum ether and ethyl acetate as eluent to give compound **5** as a white solid. Yield: 62%. ^{1}H NMR [400 MHz, dimethyl sulfoxide (DMSO)] δ 7.36 to 7.18 (m, 2H), 5.15 (s, 1H), 4.18 (q, *J* = 7.1 Hz, 4H), 1.23 to 1.14 (m, 6H). HRMS-ESI (electrospray ionization): calcd for $[C_{13}H_{13}F_3O_4 + Na]^+$ 313.0664, found: 313.0663.

General procedure for the synthesis of 5,7-dichloro-6-(2,4,6-trifluorophenyl)-[1,2,4]triazolo[1,5-a]pyrimidine (7)
A mixture of 3-amino-1,2,4-triazole (84 mg, 1.0 mmol), compound **5** (290 mg, 1.0 mmol), and tributylamine (1.0 ml) was heated at 180°C for 4 hours. After the reaction, the mixture was cooled to room temperature, and the residue was diluted with dichloromethane, washed with diluted hydrochloric acid and water, and crystallized from diisopropyl ether to yield 116 mg of compound **6** (brown solid, 41% yield). Then, phosphorus oxytrichloride (10 ml) was added to a 25-ml round-bottom flask filled with compound **6** (282 mg, 1.0 mmol) and refluxed for 4 hours. After completion of the reaction, the reaction mixture was cooled to room temperature, and the solvent was distilled off. The residue was diluted with water and ether acetate. The organic phase was separated, washed with diluted sodium bicarbonate solution and brine, dried, concentrated in vacuo, and purified by chromatography on silica gel with petroleum ether and ethyl acetate as eluent to give compound **7** as a white solid. Yield: 66%, ^{1}H NMR (400 MHz, DMSO) δ 8.90 (s, 1H), 7.62 to 7.55 (m, 2H). HRMS-ESI: calcd for $[C_{11}H_3Cl_2F_3N + H]^+$ 318.9765, 320.9736, found: 318.9764, 320.9739; calcd for $[C_{11}H_3Cl_2F_3N + Na]^+$ 340.9585, 342.9555, found: 340.9576, 342.9565.

General procedure for the synthesis of 1 and 2
Compounds **1** and **2** were prepared as described in Zhang *et al.* (*23*). Compound **7** (160 mg, 0.5 mmol), (S)-1,1,1-trifluoropropan-2-amine hydrochloride (75 mg, 0.5 mmol, for 1), or (1R,3r,5S)-3-methoxy-8-azabicyclo[3.2.1]octane (71 mg, 0.5 mmol for 2) and potassium carbonate (276 mg, 2.0 mmol) were dissolved in N,N′-dimethylformamide (5 ml) and stirred at room temperature for 4 hours. After completion of the reaction, water and ethyl acetate were added. The organic phase was separated, washed with brine, dried over anhydrous sodium sulfate, concentrated in vacuo, and purified by chromatography on silica gel with petroleum ether and ethyl acetate as eluent to give compounds **1** and **2** as white solid. Yield: 48 to 63%.

(S)-5-chloro-6-(2,4,6-trifluorophenyl)-N-(1,1,1-trifluoropropan-2-yl)-[1,2,4]triazolo[1,5-a]pyrimidin-7-amine (**1**): Yield: 48%, ^{1}H NMR (400 MHz, CDCl₃) δ 8.40 (s, 1H), 6.93 to 6.89 (m, 2H), 5.96 (d, *J* = 10.6 Hz, 1H), and 4.75 (s, 1H), 1.43 (t, *J* = 10.0 Hz, 3H). HRMS-ESI: calcd for $[C_{14}H_8ClF_6N_5 + H]^+$ 396.0451, found 396.0488; calcd for $[C_{14}H_8ClF_6N_5 + Na]^+$ 418.0270, found 418.0263.

5-Chloro-7-((1R,3r,5S)-3-methoxy-8-azabicyclo[3.2.1]octan-8-yl)-6-(2,4,6-trifluorophenyl)-[1,2,4]triazolo[1,5-a]pyrimidine (**2**): Yield: 63%, ^{1}H NMR (400 MHz, DMSO) δ 8.57 (s, 1H), 7.52 to 7.48 (m, 2H), 4.58 (s, 2H), 3.43 (t, *J* = 4.0 Hz, 1H), 3.17 (s, 3H), 2.01 (dt, *J* = 10.2, 5.1 Hz, 4H), and 1.90 (d, *J* = 14.6 Hz, 2H), 1.77 to 1.67 (m, 2H). HRMS-ESI: calcd for $[C_{19}H_{17}ClF_3N_5O + H]^+$ 424.1152, found 424.1152; calcd for $[C_{19}H_{17}ClF_3N_5O + Na]^+$ 446.0971, found 446.0964.

Cell culture
HeLa, Hct116, H460, and SU-DHL-6 cells were all sourced from the American Type Culture Collection. H460 cells were cultured in RPMI 1640 medium and HeLa, Hct116, and SU-DHL-6 cells were cultured in Dulbecco's modified Eagle's medium. Both media were supplemented with 5 to 10% fetal bovine serum and about 1% penicillin-streptomycin. The culture temperature was set at 37°C, and cells were grown in a humidified incubator with 5% CO_2. All cells have been authenticated by short tandem repeat tests and are free of mycoplasma.

Label-free quantitative proteomics

HeLa cells were treated with or without 1 μM cevipabulin for 6 hours, and then all cells were collected and lysed with radioimmuno-precipitation assay buffer (containing proteinase inhibitor mixture) for 30 min on ice. Then, all samples were centrifuged at 10,000*g* for 30 min to pellet cell debris. Supernatants were collected and stored at −80°C before analysis. We have done three biological repeats. Then, the following label-free quantitative proteomic analysis of these samples was carried out following the procedure as described previously (*13*).

Immunoblotting

Cells were plated on six-well plates and cultured for 24 hours before treated with different compounds for different times. Total cells were harvested and washed by phosphate-buffered saline (PBS) before centrifuged at 1000*g* for 3 min. Then, 1× loading buffer (diluted from 6× loading buffer by radioimmunoprecipitation assay buffer 1) was added to the cell pellets and lysed for 10 min. Samples were then incubated in boiling water for 10 min and then stored at −20°C before use. Equal volume of samples was loaded to 10% SDS–polyacrylamide gel electrophoresis for electrophoresis and then transferred to polyvinylidene difluoride (PVDF) membranes at 4°C for 2 hours. Proteins on PVDF membranes were incubated in blocking buffer [5% skim milk diluted in 1 × PBST (PBS buffer with 0.1% Tween-20)] for 1 hour. Then, the PVDF membranes were incubated with first antibodies (diluted in blocking buffer) for 12 hours and washed three times with PBST before incubating with second antibody (diluted in blocking buffer) for 45 min and washed three times with PBST again. Last, the PVDF membranes were immersed in enhanced chemiluminescence reagents for 30 s subjected to image with a chemiluminescence image analysis system (Tianneng, China).

Quantitative-PCR

HeLa and Hct116 cells were plated on six-well plates and culture for 24 hours before treated with cevipabulin for different times. Total mRNA of both HeLa and Hct116 cells was extracted with TRIzol (Invitrogen, USA) agents following the manufacturer's protocol and then qualified using a NanoDrop1000 spectrophotometer (Thermo Fisher Scientific, USA). The cDNA synthesis was carried out using a High-Capacity cDNA Reverse Transcription Kit (Applied Biosystems, USA). Taq Universal SYBR Green Supermix (Bio-Rad, USA) was used for further quantitative-PCR analysis on a CFX96 Real-time PCR System (Bio-Rad, USA). Relative mRNA levels of both α-tubulin and β-tubulin were normalized to that of GAPDH. The primers used were as follows:

α-tubulin: forward primer, TCGATATTGAGCGTCCAACCT; reverse primer, CAAAGGCACGTTTGGCATACA;

β-tubulin: forward primer, TGGACTCTGTTCGCTCAGGT; reverse primer, TGCCTCCTTCCGTACCACAT;

GAPDH: forward primer, GGAGCGAGATCCCTCCAAAAT; reverse primer, GGCTGTTGTCATACTTCTCATGG.

Single amino acid substitution on α-tubulin

The pIRESneo-EGFP (enhanced green fluorescent protein)–α-tubulin plasmid was obtained from Addgene (USA), and mutation (Y224G) of α-tubulin was performed using a Q5 Site-Directed Mutagenesis kit (NEB no. E0554S, USA). HeLa cells were plated on six-well plates and incubated for 24 hours before transfected with these plasmids by Lipofectamine 2000. Then, the cells were cultured for

another 24 hours before treated with or without different compounds for 16 hours. Total protein was extracted and analyzed by immunoblotting to detect the content of GTP-α-tubulin, and GAPDH was used as loading control.

Stoichiometry of cevipabulin or compound 1 to tubulin dimer

Tubulin (20 μM) in Pipes buffer [80 mM Pipes (pH 6.9), 0.5 mM EGTA, and 2 mM MgCl₂] supplemented with 1 mM GTP were incubated with cevipabulin (8, 16, 32, 64, 128, or 256 μM) or compound **1** (2, 4, 8, 16, 32, or 64 μM) for 10 min. Then, the unbounded compounds were washed away with an ultrafiltration method (centrifugated three times in a 10-kDa ultrafiltration tube at 13,000 rpm for 5 min). The retentate (tubulin) was heated to 90°C for 5 min to denature the tubulin protein and release the bound cevipabulin. The bound cevipabulin was quantified with an LC-MS/MS.

Stoichiometry of cevipabulin to eribulin preincubated tubulin dimer

Tubulin (1 μM) in Pipes buffer [80 mM Pipes (pH 6.9), 0.5 mM EGTA, and 2 mM MgCl₂] supplemented with 1 mM GTP were incubated with 1.5 μM eribulin for 10 min and then concentrated to 20 μM before further incubated with 6, 12, 24, 48, or 96 μM cevipabulin for another 10 min. Then, the unbounded compounds were washed with an ultrafiltration method (centrifugated three times in a 10-kDa ultrafiltration tube at 13,000 rpm for 5 min). The retentate (tubulin) was heated to 90°C for 5 min to denature the tubulin protein and release the bound compounds. The bound cevipabulin and eribulin were quantified with LC-MS/MS.

LC-MS/MS method

LC-MS/MS analysis was performed on an ultrafast liquid chromatography system (Shimadzu) coupled with an AB SCIEX Qtrap 5500 mass spectrometer, equipped with ESI source. Instrument control and collection of chromatographic and mass spectrometry information were carried out by analyst 1.6.2 software (AB SCIEX, USA). Chromatographic separation was achieved on a Waters ACQUITY UPLC BEH C₁₈ column (2.1 mm × 100 mm inside diameter, 1.7 μm). The mobile phase system consisted of 0.1% formic acid in water (A) and acetonitrile (B) using a gradient elution as follows: 0 to 1.0 min, 10 to 90% B; held 90% B for 1 min. The flow rate was 0.5 ml/min, and the temperature of the column and autosampler was maintained at 35° and 15°C, respectively. The injection volume was 1 μl. In the MS analysis, positive ionization mode was used for sample detection, with the following optimized mass spectrometric parameters: ionspray voltage, 5500 V; declustering potential, 100 V; and temperature, 500°C. Eribulin, compound **1**, cevipabulin, and IS were conducted in multireaction monitoring mode with ion pairs of 730.4 > 680.4, 396.0 > 360.1, 465.0 > 358.2, and 265.2 > 232.2, respectively.

MST assay

Binding of cevipabulin or compound **1** to the seventh site was detected with an MST assay with a Monolith NT.115 instrument (NanoTemper Technologies). Purified tubulin was labeled using the Monolith protein labeling kit RED-NHS (NanoTemper Technologies) and then diluted to 200 nM concentration before incubated with 2 μM eribulin for 20 min at room temperature. Different concentrations of cevipabulin (20 μM to 48.9 nM) or compound **1**

(200 μM to 12.2 nM) were incubated with labeled tubulin (100 nM) in assay buffer [80 mM Pipes, (pH 6.9), 0.5 mM EGTA, 2 mM MgCl$_2$, and 1 mM GTP] for 10 min at 4°C. Samples were loaded into glass capillaries for detection. K_d values were obtained using Nano-Temper software.

Determination of the K_d of cevipabulin to vinblastine site by competition assay
Different concentrations of BODIPY-Vinblastine (50 μM to 48.9 nM) were incubated with 50 nM tubulin dimer and RB3 (T2R) complex (2:1.2) plus with 1% DMSO or 50 μM vinblastine (final DMSO concentration was 1%) for 10 min. The fluorescent emission ratio (520/490 nm, 340 nm excitation) was detected using a BioTek Gen5 spectrophotometer (BioTek, USA). The data of each concentration were calculated as Data$_{DMSO}$ − Data$_{Vinblastine}$. The specific equilibrium binding constant (K_d) was obtained by fitting the data into a one-site specific binding equation using GraphPad Prism 5.0. The K_d value was determined to be 1.571 ± 0.23 μM. The T2R complex (50 nM) was preincubated with 1 μM BODIPY-vinblastine for 10 min before further incubation with different concentrations of cevipabulin for another 10 min. Next, fluorescence emission was determined at 520/490 nm (340 nm excitation). The data were fit into a one-site competitive binding equation in a dose-dependent manner to obtain IC$_{50}$ values. The inhibition constant (K_i) value was calculated using the following equation (24)

$$K_i = IC_{50}/(1 − [L]/KL)$$

IC$_{50}$ is the concentration of cevipabulin that inhibits 50% of binding, [L] is the concentration of BODIPY-vinblastine (1000 nM), and KL is the K_d value of BODIPY-vinblastine to T2R (1571 nM).

Structural biology
Protein expression and purification were described in detail in our precious study (25). Tubulin, RB3, and TTL (2:1.3:1.2 molar ratio) were mixed together, then 5 mM tyrosine, 10 mM DTT, and 1 mM AMPPCP were added, and then the mixture was concentrated to about 15 mg/ml at 4°C. The crystallization is conducted using a sitting-drop vapor-diffusion method under 20°C, and the crystallization buffer is optimized as 6% polyethylene glycol 4000, 8% glycerol, 0.1 M MES (pH 6.7), 30 mM CaCl$_2$, and 30 mM MgCl$_2$. Seeding method was also used to obtain single crystals. Crystals appeared in about 2 days and in a rod-like shape, and the size reached maximum dimensions within 1 week.

About 0.1 μl of cevipabulin (diluted in DMSO with a concentration of 100 mM) was added to a drop containing tubulin crystal and incubated for 16 hours at 20°C to obtain the cevipabulin-tubulin complex. About 0.1 μl of cevipabulin (100 mM) and 0.1 μl of eribulin (100 mM) were added to a drop containing tubulin crystal and incubated for 16 hours at 20°C to obtain the cevipabulin-eribulin-tubulin complex. The following data collection and structure determination were the same as previously described (25).

TPE-MI as a thiol probe to detect unfolded protein
TPE-MI is a small molecule that is inherently nonfluorescent until it covalently binds to a thiol by its maleimide (21, 26). This molecule could be used to monitor purified protein unfolding in vitro (21). Purified tubulin (0.2 mg/ml) was diluted in Pipes buffer supplemented with 1 mM GTP and then mixed with 50 μM TPE-MI and

different compounds for various times. Then, the samples were immediately subjected to a microplate reader (BioTek, USA) to detect the fluorescence (excitation wavelength: 350 nm; emission wavelength: 470 nm).

Quantification of tubulin-bound GTP and GDP
Tubulin (20 μM) in Pipes buffer supplemented with 1 mM GDP was incubated with cevipabulin (30 μM), compound **1** (30 μM), compound **2** (30 μM), or vinblastine (30 μM) for 10 min, and then tubulin was washed three times with Pipes buffer in a 10-kDa ultrafiltration tube. The retentate (tubulin) was heated to 90°C for 5 min to denature the tubulin protein and release the bound GTP and GDP, which was further quantified with an LC-MS/MS method. Tubulin (20 μM) in Pipes buffer supplemented with 1 mM GDP was incubated with cevipabulin (30 μM), compound **1** (30 μM), compound **2** (30 μM), or vinblastine (30 μM) for 10 min, and then the tubulin was washed three times with Pipes buffer in a 10-kDa ultrafiltration tube. The retentate (tubulin) was heated to 90°C for 5 min to denature the tubulin protein and release the bound GTP and GDP, which was further quantified with an LC-MS/MS method.

Statistical analysis
Data are presented as means. Statistical differences were determined using an unpaired Student's t test. P values are indicated in the figure legend when necessary: * or #, $P < 0.05$.

SUPPLEMENTARY MATERIALS
Supplementary material for this article is available at http://advances.sciencemag.org/cgi/content/full/7/21/eabg4168/DC1

View/request a protocol for this paper from *Bio-protocol*.

REFERENCES AND NOTES
1. K. E. Arnst, S. Banerjee, H. Chen, S. Deng, D. J. Hwang, W. Li, D. D. Miller, Current advances of tubulin inhibitors as dual acting small molecules for cancer therapy. *Med. Res. Rev.* **39**, 1398–1426 (2019).
2. K. Haider, S. Rahaman, M. S. Yar, A. Kamal, Tubulin inhibitors as novel anticancer agents: An overview on patents (2013-2018). *Expert Opin. Ther. Pat.* **29**, 623–641 (2019).
3. B. Gigant, C. Wang, R. B. Ravelli, F. Roussi, M. O. Steinmetz, P. A. Curmi, A. Sobel, M. Knossow, Structural basis for the regulation of tubulin by vinblastine. *Nature* **435**, 519–522 (2005).
4. H. Doodhi, A. E. Prota, R. Rodríguez-García, H. Xiao, D. W. Custar, K. Bargsten, E. A. Katrukha, M. Hilbert, S. Hua, K. Jiang, I. Grigoriev, C.-P. H. Yang, D. Cox, S. B. Horwitz, L. C. Kapitein, A. Akhmanova, M. O. Steinmetz, Termination of protofilament elongation by eribulin induces lattice defects that promote microtubule catastrophes. *Curr. Biol.* **26**, 1713–1721 (2016).
5. J. Yang, Y. Wang, T. Wang, J. Jiang, C. H. Botting, H. Liu, Q. Chen, J. Yang, J. H. Naismith, X. Zhu, L. Chen, Pironetin reacts covalently with cysteine-316 of α-tubulin to destabilize microtubule. *Nat. Commun.* **7**, 12103 (2016).
6. M. Kavallaris, Microtubules and resistance to tubulin-binding agents. *Nat. Rev. Cancer* **10**, 194–204 (2010).
7. A. E. Prota, J. Setter, A. B. Waight, K. Bargsten, J. Murga, J. F. Diaz, M. O. Steinmetz, Pironetin binds covalently to αCys316 and perturbs a major loop and helix of α-tubulin to inhibit microtubule formation. *J. Mol. Biol.* **428**, 2981–2988 (2016).
8. A. E. Prota, K. Bargsten, D. Zurwerra, J. J. Field, J. F. Díaz, K.-H. Altmann, M. O. Steinmetz, Molecular mechanism of action of microtubule-stabilizing anticancer agents. *Science* **339**, 587–590 (2013).
9. A. E. Prota, K. Bargsten, P. T. Northcote, M. Marsh, K. H. Altmann, J. H. Miller, J. F. Díaz, M. O. Steinmetz, Structural basis of microtubule stabilization by laulimalide and peloruside A. *Angew. Chem. Int. Ed.* **53**, 1621–1625 (2014).
10. R. B. Ravelli, B. Gigant, P. A. Curmi, I. Jourdain, S. Lachkar, A. Sobel, M. Knossow, Insight into tubulin regulation from a complex with colchicine and a stathmin-like domain. *Nature* **428**, 198–202 (2004).
11. A. E. Prota, K. Bargsten, J. F. Diaz, M. Marsh, C. Cuevas, M. Liniger, C. Neuhaus, J. M. Andreu, K.-H. Altmann, M. O. Steinmetz, A new tubulin-binding site

and pharmacophore for microtubule-destabilizing anticancer drugs. *Proc. Natl. Acad. Sci. U.S.A.* **111**, 13817–13821 (2014).

12. M. L. Antony, J. Lee, E. R. Hahm, S. H. Kim, A. I. Marcus, V. Kumari, X. Ji, Z. Yang, C. L. Vowell, P. Wipf, G. T. Uechi, N. A. Yates, G. Romero, S. N. Sarkar, S. V. Singh, Growth arrest by the antitumor steroidal lactone withaferin A in human breast cancer cells is associated with down-regulation and covalent binding at cysteine 303 of β-tubulin. *J. Biol. Chem.* **289**, 1852–1865 (2014).

13. J. Yang, Y. Li, W. Yan, W. Li, Q. Qiu, H. Ye, L. Chen, Covalent modification of Cys-239 in β-tubulin by small molecules as a strategy to promote tubulin heterodimer degradation. *J. Biol. Chem.* **294**, 8161–8170 (2019).

14. S. Ayral-Kaloustian, N. Zhang, C. Beyer, Cevipabulin (TTI-237): Preclinical and clinical results for a novel antimicrotubule agent. *Methods Find. Exp. Clin. Pharmacol.* **31**, 443–447 (2009).

15. C. F. Beyer, N. Zhang, R. Hernandez, D. Vitale, J. Lucas, T. Nguyen, C. Discafani, S. Ayral-Kaloustian, J. J. Gibbons, TTI-237: A novel microtubule-active compound with in vivo antitumor activity. *Cancer Res.* **68**, 2292–2300 (2008).

16. J. Kovalevich, A.-S. Cornec, Y. Yao, M. James, A. Crowe, V. M.-Y. Lee, J. Q. Trojanowski, A. B. Smith, C. Ballatore, K. R. Brunden, Characterization of brain-penetrant pyrimidine-containing molecules with differential microtubule-stabilizing activities developed as potential therapeutic agents for Alzheimer's disease and related tauopathies. *J. Pharmacol. Exp. Ther.* **357**, 432–450 (2016).

17. G. Sáez-Calvo, A. Sharma, F. de Asís Balaguer, I. Barasoain, J. Rodríguez-Salarichs, N. Olieric, H. Muñoz-Hernández, M. Á. Berbís, S. Wendeborn, M. A. Peñalva, R. Matesanz, Á. Canales, A. E. Prota, J. Jímenez-Barbero, J. M. Andreu, C. Lamberth, M. O. Steinmetz, J. F. Díaz, Triazolopyrimidines are microtubule-stabilizing agents that bind the Vinca inhibitor site of tubulin. *Cell Chem. Biol.* **24**, 737–750.e6 (2017).

18. C. F. Beyer, N. Zhang, R. Hernandez, D. Vitale, T. Nguyen, S. Ayral-Kaloustian, J. J. Gibbons, The microtubule-active antitumor compound TTI-237 has both paclitaxel-like and vincristine-like properties. *Cancer Chemother. Pharmacol.* **64**, 681–689 (2009).

19. M. Menéndez, G. Rivas, J. F. Díaz, J. M. Andreu, Control of the structural stability of the tubulin dimer by one high affinity bound magnesium ion at nucleotide N-site. *J. Biol. Chem.* **273**, 167–176 (1998).

20. B. M. Spiegelman, S. M. Penningroth, M. W. Kirschner, Turnover of tubulin and the N site GTP in Chinese hamster ovary cells. *Cell* **12**, 587–600 (1977).

21. M. Z. Chen, N. S. Moily, J. L. Bridgford, R. J. Wood, M. Radwan, T. A. Smith, Z. Song, B. Z. Tang, L. Tilley, X. Xu, G. E. Reid, M. A. Pouladi, Y. Hong, D. M. Hatters, A thiol probe for measuring unfolded protein load and proteostasis in cells. *Nat. Commun.* **8**, 474 (2017).

22. D. A. Keays, G. Tian, K. Poirier, G.-J. Huang, C. Siebold, J. Cleak, P. L. Oliver, M. Fray, R. J. Harvey, Z. Molnár, M. C. Piñon, N. Dear, W. Valdar, S. D. M. Brown, K. E. Davies, J. N. P. Rawlins, N. J. Cowan, P. Nolan, J. Chelly, J. Flint, Mutations in α-tubulin cause abnormal neuronal migration in mice and lissencephaly in humans. *Cell* **128**, 45–57 (2007).

23. N. Zhang, S. Ayral-Kaloustian, T. Nguyen, J. Afragola, R. Hernandez, J. Lucas, J. Gibbons, C. Beyer, Synthesis and SAR of [1, 2, 4] triazolo [1, 5-a] pyrimidines, a class of anticancer agents with a unique mechanism of tubulin inhibition. *J. Med. Chem.* **50**, 319–327 (2007).

24. C. Yung-Chi, W. H. Prusoff, Relationship between the inhibition constant (KI) and the concentration of inhibitor which causes 50 per cent inhibition (I50) of an enzymatic reaction. *Biochem. Pharmacol.* **22**, 3099–3108 (1973).

25. L. Niu, J. Yang, W. Yan, Y. Yu, Y. Zheng, H. Ye, Q. Chen, L. Chen, Reversible binding of the anticancer drug KXO1 (tirbanibulin) to the colchicine-binding site of β-tubulin explains KXO1's low clinical toxicity. *J. Biol. Chem.* **294**, 18099–18108 (2019).

26. Y. Liu, Y. Yu, J. W. Lam, Y. Hong, M. Faisal, W. Z. Yuan, B. Z. Tang, Simple biosensor with high selectivity and sensitivity: Thiol-specific biomolecular probing and intracellular imaging by AIE fluorogen on a TLC plate through a thiol–ene click mechanism. *Chemistry* **16**, 8433–8438 (2010).

Citation: J. Yang, Y. Yu, Y. Li, W. Yan, H. Ye, L. Niu, M. Tang, Z. Wang, Z. Yang, H. Pei, H. Wei, M. Zhao, J. Wen, L. Yang, L. Ouyang, Y. Wei, Q. Chen, W. Li, L. Chen, Cevipabulin-tubulin complex reveals a novel agent binding site on α-tubulin with tubulin degradation effect. *Sci. Adv.* **7**, eabg4168 (2021).